NASA TECHNICAL NOTE

NASA TN D-5986

NATURAL VIBRATION AND FLUTTER OF ELASTICALLY SUPPORTED CORRUGATION-STIFFENED PANELS – EXPERIMENT AND THEORY

by Walter L. Heard, Jr., and Herman L. Bohon

Langley Research Center
Hampton, Va. 23365

NATIONAL AERONAUTICS AND SPACE ADMINISTRATION • WASHINGTON, D. C. • OCTOBER 1970

1. Report No.	2. Government Accession No.	3. Recipient's Catalog No.
NASA TN D-5986		

4. Title and Subtitle	5. Report Date
NATURAL VIBRATION AND FLUTTER OF ELASTICALLY SUPPORTED CORRUGATION-STIFFENED PANELS – EXPERIMENT AND THEORY	October 1970
	6. Performing Organization Code
7. Author(s)	8. Performing Organization Report No.
Walter L. Heard, Jr., and Herman L. Bohon	L-6772
	10. Work Unit No.
9. Performing Organization Name and Address	126-14-14-06
NASA Langley Research Center Hampton, Va. 23365	11. Contract or Grant No.
	13. Type of Report and Period Covered
12. Sponsoring Agency Name and Address	Technical Note
National Aeronautics and Space Administration Washington, D.C. 20546	14. Sponsoring Agency Code

15. Supplementary Notes

16. Abstract

The natural vibration and flutter characteristics of two corrugation-stiffened panels were studied experimentally and theoretically to determine the effects of finite deflectional, rotational, and torsional stiffnesses of the boundary supports. Flutter tests were conducted at a Mach number of 3. The experimental data are compared with results from a flutter theory for orthotropic panels which includes the effects of finite support stiffnesses as well as uniform in-plane loading of the panel.

The investigation indicates that finite deflectional, rotational, and torsional stiffnesses of the boundary supports must be accounted for in the theory in order to match experimental natural frequencies of the test panels. However, it is concluded that structural damping (neglected in the theory) strongly influenced the flutter behavior of the test panels. Furthermore, the theory shows that the addition of torsional stiffening at the supports is a definite asset for increasing flutter dynamic pressure and may be extremely important in the design of panels for application at hypersonic speeds where thermal expansion may be desired.

17. Key Words (Suggested by Author(s))	18. Distribution Statement
Panel flutter Natural vibration of panels Orthotropic panels on flexible supports	Unclassified – Unlimited

19. Security Classif. (of this report)	20. Security Classif. (of this page)	21. No. of Pages	22. Price*
Unclassified	Unclassified	36	$3.00

*For sale by the Clearinghouse for Federal Scientific and Technical Information
Springfield, Virginia 22151

NATURAL VIBRATION AND FLUTTER OF ELASTICALLY SUPPORTED CORRUGATION-STIFFENED PANELS – EXPERIMENT AND THEORY

By Walter L. Heard, Jr., and Herman L. Bohon
Langley Research Center

SUMMARY

The natural vibration and flutter characteristics of two corrugation-stiffened panels were studied experimentally and theoretically to determine the effects of finite deflectional, rotational, and torsional stiffnesses of the boundary supports. Flutter tests were conducted at a Mach number of 3 in the Langley 9- by 6-foot thermal structures tunnel. The test specimens were restrained against in-plane thermal expansion in the streamwise direction; thus, uniform in-plane loading was induced by aerodynamic heating. The experimental flutter data are compared with flutter theory for orthotropic panels (developed in the present report) which includes the effects of finite support stiffnesses as well as uniform in-plane loading of the panel. The panel support stiffnesses (determined from experimental natural frequencies) and an assumed state of stress are used in the theory for comparison with the flutter data. The investigation indicates that finite deflectional, rotational, and torsional stiffnesses of the boundary supports must be accounted for in the theory in order to match experimental natural frequencies of the test panels. However, it is concluded that structural damping (neglected in the theory) strongly influenced the flutter behavior of the test panels. Furthermore, the theory shows that the addition of torsional stiffening at the supports is a definite asset for increasing flutter dynamic pressure and may be extremely important in the design of panels for application at hypersonic speeds where free thermal expansion may be desired.

INTRODUCTION

Current designs of hypersonic vehicles indicate that exterior surfaces may consist essentially of corrugation-stiffened panels with flexible boundary supports. Such supports may be designed to allow essentially free in-plane thermal expansion of the panels; thus, buildup of large thermal stresses due to boundary restraints can be prevented. Panel flutter characteristics, however, may be adversely affected by flexible supports unless careful attention is given to the design of the supports. (See ref. 1.)

In reference 2 early experimental flutter data for corrugation-stiffened panels are compared with theory for orthotropic panels; the experimental values for flutter dynamic

pressure are found to be very much lower than those predicted by the theory. This discrepancy is attributed to the assumption, in the theory, of infinite deflectional stiffness of the supports at the ends of the corrugations. Reference 3 shows that if the supports are assumed to have finite deflectional stiffness, the agreement of theory with experiment is greatly improved; nevertheless, significant differences remain (ref. 4). In the theory of reference 3, however, torsional support stiffness is assumed to be zero, rotational support stiffness is assumed to be either zero or infinite, and panel in-plane loading is neglected. Thus, the objectives of the present paper are (1) to provide experimental natural vibration and flutter data when the effects of the boundary support stiffnesses and in-plane loading of the panel may be important considerations and (2) to provide a more complete orthotropic-panel flutter theory by adding effects of finite torsional and rotational stiffnesses and uniform in-plane loading to the theory of reference 3.

Experimental flutter characteristics are presented for two thermally stressed corrugation-stiffened panels. Both panels were tested with the corrugations alined normal to the airstream. The leading and trailing edges of the panels were essentially simply supported. The side (streamwise) edges of the panels were attached to finite-stiffness supports designed to permit simple calculations of deflectional and rotational stiffnesses. The torsional stiffnesses of the supports were determined by correlating measured natural frequencies of the panels with theory. After the natural frequencies were measured, flutter tests were conducted at a Mach number of 3 in the Langley 9- by 6-foot thermal structures tunnel. The test specimens were restrained against thermal expansion in the streamwise direction; thus, uniform in-plane loading was induced by aerodynamic heating. Results are presented in the form of plots of the critical dynamic-pressure parameter as a function of change in panel temperature.

The flutter theory for stressed orthotropic panels presented herein accounts for the finite deflectional, rotational, and torsional stiffnesses of the boundary supports at the ends of the corrugations. The other two edges are assumed to be simply supported. The effects of the various spring supports are discussed and theoretical flutter mode shapes are presented. The experimental data are compared with flutter boundaries predicted by the theory by using an assumed state of stress.

SYMBOLS

The units used for the physical quantities in this paper are given both in the U.S. Customary Units and in the International System of Units (SI). Factors relating the two systems are given in reference 5, and those used in the present investigation are presented in appendix A.

A amplitude coefficient

$\overline{A}_{y,m}$ quantity defined in equation (B9)

a panel length (x-direction)

$\overline{B}_{y,m}$ frequency parameter (see eq. (B8))

b panel width (y-direction)

C_m, D_m constants of integration

$$D_1 = \frac{D_x}{1 - \mu_x \mu_y}$$

$$D_2 = \frac{D_y}{1 - \mu_x \mu_y}$$

$$D_{12} = D_{xy} + \mu_x D_2$$

D_x, D_y panel bending stiffnesses in x- and y-directions, respectively

D_{xy} panel twisting stiffness

d width of beam spring

E Young's modulus

$$\overline{E} = \frac{EI}{hD_2}$$

f frequency

h distance between beam springs (see fig. 2(a))

I moment of inertia of spring cross section

K_D, K_R, K_T deflectional, rotational, and torsional spring constants, respectively, per unit length

$\overline{K}_D, \overline{K}_R, \overline{K}_T$ nondimensional deflectional, rotational, and torsional spring constants, respectively (see eqs. (B13))

l	effective length of beam spring
M	Mach number
m,n	number of half-waves in streamwise direction
N_x, N_y	uniform in-plane loads per unit length in x- and y- directions, respectively
$N_{x,cr}$	in-plane buckling load at flutter
q	dynamic pressure of airstream
q_{cr}	dynamic pressure of airstream at flutter
ΔT	change in average temperature of panel cover sheet
t	thickness of support spring
w	lateral deflection of panel
x,y	Cartesian coordinates of panel
Y_m, Y_n	function describing shape of natural mode of vibration in y-direction (see eqs. (B6) and (B10))
γ	mass per unit area of panel
ϵ, δ	parameters associated with characteristic roots (see eqs. (B11))
λ	dynamic-pressure parameter, $\frac{2qa^3}{D_1\sqrt{M^2 - 1}}$
λ_{cr}	dynamic-pressure parameter at flutter
μ	Poisson's ratio
μ_x, μ_y	Poisson's ratio associated with curvature in y- and x- directions, respectively
τ	time

ω circular frequency

ω_r fundamental frequency of simply supported beam (radians per sec), $(\pi^2/a^2)\sqrt{D_1/\gamma}$

Subscript:

ref reference value

TEST APPARATUS

Panels

Two corrugation-stiffened panels were constructed for the present tests according to the construction details shown in figure 1. The panels were identical except that for panel I, $a/b = 1/2$, and for panel II, $a/b = 1$. The width b of each panel was 20 inches (50.8 cm). The panels, consisting of a corrugated sheet and a flat cover sheet (external skin), were fabricated from René 41. The corrugated sheet thickness was 0.010 inch (0.025 cm). The flat cover sheet 0.007 inch (0.018 cm) thick, was spotwelded at approximately 0.25-inch (0.64-cm) intervals along the length of each corrugation (two rows of welds per corrugation). The cover sheet provided a relatively smooth aerodynamic surface. A René 41 doubler strap, 0.60 inch (1.52 cm) wide and 0.030 inch (0.076 cm) thick (consisting of three 0.010-inch-thick (0.025-cm) straps), was seamwelded to each of the streamwise edges of the corrugation sheet prior to forming; the sheet and straps were then formed simultaneously. The straps, which were treated as part of the boundary supports and not as part of the panel, strengthened the spring-supported edges of the panel for mounting purposes and provided a source of torsional stiffness. At the leading and trailing edges, formed aluminum channel section supports were attached to the panels as shown in detail A of figure 1. These channels were 1.70 inches (4.32 cm) deep and 0.050 inch (0.127 cm) thick. Each channel was attached to the panel by a single row of rivets. The panel stiffness parameters D_1, D_2, and D_{xy} (identical for the two panels) were calculated by use of the method in reference 6 and are given in table I.

Support Springs and Mounting Arrangements

The support springs and the mounting arrangements for the streamwise edges and the leading and trailing edges are shown in figure 2. Two sets of springs (fig. 2(a)) were machined from blued shim stock so that when the panels were mounted, the ends of each corrugation of the panel rested on a small cantilever beam spring. The spring thickness was 0.015 inch (0.038 cm) for the rectangular panel, and 0.029 inch (0.074 cm) for the

square panel. The width of each beam spring was 0.50 inch (1.27 cm); the effective length l was assumed to be 1.26 inches (3.20 cm), the distance between center lines of the attachment holes. The spring spacing h was 1.00 inch (2.54 cm). A view of a streamwise edge of a panel showing the corrugations, doubler strap, and hole for attaching the spring is shown in figure 2(b). Figure 2(c) shows the streamwise-edge support arrangement. Small aluminum blocks were used as spacers between the spring and the panel corrugations to aline the flat surface of the panel flush with the aerodynamic surface of the test-section panel holder. These blocks were chamfered as shown to minimize changes in rotational restraint of the springs between upward and downward movement of the panel edges. Each beam spring was attached to its corresponding corrugation by a single machine screw and an aluminum block which was drilled and tapped and inserted into the ends of the corrugations. The support arrangement for the leading and trailing edges is shown in figure 2(d).

The panels were mounted in a flat-sided steel panel holder (figs. 3 and 4), which extended vertically through the test section. The panel holder has a beveled half-wedge leading edge with a cavity on the nonbeveled side 5.0 inches (12.7 cm) deep, 29.00 inches (73.6 cm) in the direction of airflow, and 30 inches (76 cm) high. The cavity, which is located 26.50 inches (67.3 cm) downstream from the leading edge, is used for accommodating test specimens. The panel holder is equipped with pneumatic, vertically operating sliding doors which cover the cavity area to protect the test specimens during tunnel start and shutdown. Aerodynamic fences attached to the doors insure essentially free-stream flow conditions over the cavity area. The pressure inside the cavity and behind the test specimen is controlled by a vent-door arrangement on the side of the panel holder opposite the panel. The test panels were attached to a mounting frame which was inserted in the cavity. A test panel mounted in the panel holder in the wind-tunnel test section is shown in figure 4. The view is from upstream and the protective doors are shown fully opened.

Instrumentation

Five iron-constantan thermocouples spotwelded to each of the panel cover sheets at the locations shown in figure 5 were used to measure cover-sheet temperatures during the flutter tests. Three variable reluctance-type deflectometers were located behind the panel in the panel-holder cavity to detect panel motion and to obtain flutter frequencies. The locations of the deflectometers are also indicated in figure 5. All wind-tunnel tests were monitored with high-speed 16-mm motion pictures to detect panel motion. The exposed surface of each panel was painted with a grid for photographic purposes. (See fig. 4.)

Static pressures in the tunnel and at several locations on the panel holder and in the cavity behind the panel were measured by quick-response strain-gage-type pressure

transducers. Tunnel stagnation pressures were obtained from static pressures measured in the settling chamber. Stagnation temperatures were measured by total-temperature probes in the test section. All pressure and temperature data were recorded on magnetic tape. Deflectometer output, which was monitored during each test, was recorded on oscillographs.

Wind Tunnel

The tests were made at a Mach number of 3 in the Langley 9- by 6-foot thermal structures tunnel, an intermittent blowdown wind tunnel which exhausts to the atmosphere. A heat exchanger is preheated to provide stagnation temperatures ranging from approximately 300° to 660° F (422 to 622 K) and dynamic pressures ranging from 1500 to 5000 lbf/ft^2 (72 to 239 kN/m^2). Run times are limited to less than a minute. For more details regarding this facility and its operation, see reference 7.

TEST PROCEDURE

Natural frequencies of each panel were measured immediately prior to each flutter test. All natural-vibration tests were conducted at ambient temperature and pressure in the tunnel test section with the panels mounted in the panel holder. The panels were vibrated with an airjet shaker, which is described in detail in reference 8.

All flutter tests were conducted at a Mach number of 3.0, dynamic pressures ranging from 1500 to 5000 lbf/ft^2 (72 to 239 kN/m^2), and stagnation temperatures ranging from 303° to 452° F (424 to 506 K). For each test, the stagnation temperature was maintained essentially constant; whereas the dynamic pressure was often varied in an attempt to either start or stop flutter. The usual test procedure consisted of establishing test conditions and then exposing the panel to the airflow by opening the protective doors. The initial test conditions were maintained for an established period of time (usually about 15 to 20 seconds) to allow the thermal stresses resulting from aerodynamic heating of the panel to initiate flutter. The dynamic pressure was then lowered in an attempt to stop flutter. If, however, flutter did not occur, the dynamic pressure was increased until flutter was observed and then lowered again (time permitting) to obtain a flutter stop point. The maximum duration of a test was approximately 45 seconds.

RESULTS AND DISCUSSION

Experiments

Vibration.- Immediately prior to each flutter test, the natural frequencies corresponding to 1 half-wave in the cross-stream direction and m half-waves in the

streamwise direction were measured. The measured frequencies for each mode were averaged for all the tests of a given panel, and the average values and deviations from the average are given in table II.

Flutter.- Four flutter tests of each panel were made for this investigation. During each test the pressure inside the panel-holder cavity was controlled so that the differential pressure across the panel was normally very close to zero and never more than ± 0.01 lbf/in^2 (69 N/m^2). Flutter was observed in all tests except one test for panel I. Pertinent tunnel and panel data at flutter for all tests are listed in table III. The data are also presented in figure 6 in plots of the nondimensional flutter parameter λ_{cr} as a function of the change in average temperature of the panel. The open symbols in figure 6 represent the start of flutter; the solid symbols represent flutter stop points, which were obtained by decreasing dynamic pressure after flutter was established. For a typical test, a tunnel stagnation pressure was preselected. The tunnel was started and was allowed to reach steady flow conditions. The protective doors of the panel holder were then opened, and the panel was exposed to the flow and aerodynamic heating. Thermal expansion of the panel was restricted by the boundary supports; thus as the panel temperature increased, thermal stresses were built up and eventually caused the panel to flutter. The dynamic pressure was then decreased (which, for two tests of panel I, was also accompanied by a slight decrease in panel temperature) until flutter ceased or the test was terminated. Flutter stop points were not obtained in all tests, however, because of the time limit involved for the blowdown wind tunnel.

Segments of the flutter boundary for each panel are represented by the solid curves faired through the most conservative experimental flutter start points shown in figure 6. For comparison with theory, the flutter dynamic pressure at zero in-plane load is determined by a linear extrapolation of the curve to $\Delta T = 0$. This extrapolation procedure has often been used with good results for aerodynamically heated isotropic and orthotropic panels. As can be seen in the figure, the linear extrapolation yields $\lambda_{cr} = 4000$ for panel I and $\lambda_{cr} = 20\,000$ for panel II. However, using the linear extrapolation procedure on the data obtained in the investigation probably does not give the correct results, as will be discussed subsequently.

Comparison With Theory

In order to have a more complete theory for comparison with the experimental data, the flutter theory of reference 3 for orthotropic panels (simply supported at the leading and trailing edges) is modified to include a torsional spring constant K_T and a rotational spring constant K_R along the lateral edges, and uniform in-plane loads N_x and N_y. The panel configuration and the spring support system are shown in figure 7; the details of

modifications to the theory are presented in appendix B. Converged vibration and flutter results were obtained by utilizing up to 40 modes in the analysis.

Spring constants.- Calculated nondimensional deflectional and rotational spring constants $\overline{K}_D$ and $\overline{K}_R$ (see eqs. (B13)), respectively, were obtained by simple strength-of-materials methods applied to the idealized structure shown in figure 8. Note that the eccentricity of the beam springs to the panel neutral surface was neglected. The elements representing the beam springs had a stiffness corresponding to EI and were assumed to be clamped at the boundaries. The element representing the panel had a stiffness corresponding to D_2 per unit length. By applying conditions of continuity of deflection, slope, moment, and shear at the spring-panel juncture, the following expressions for $\overline{K}_D$ and $\overline{K}_R$ were obtained:

$$\overline{K}_D = \frac{12\overline{E}}{\pi^3}\left(\frac{b}{l}\right)^3\left[\frac{1}{\frac{b}{l}\left(\frac{3\frac{l}{b}+1}{\frac{2}{\overline{E}}\frac{l}{b}+1}\right)+1}\right] \tag{1}$$

$$\overline{K}_R = \frac{\overline{E}}{\pi}\frac{b}{l}\left[\frac{\frac{6}{\overline{E}}\left(\frac{l}{b}\right)^2 - 1}{3\frac{l}{b}+1}\right] \tag{2}$$

where $\overline{E} = \frac{EI}{hD_2}$.

By using these equations, the results are $\overline{K}_D = 0.918$ and $\overline{K}_R = 0.098$ for panel I and $\overline{K}_D = 4.33$ and $\overline{K}_R = 0.081$ for panel II.

Because of the nature of the support system, the nondimensional torsional spring constants are difficult to evaluate. Therefore, these constants were obtained from the measured natural frequencies. However, a lower limit of $\overline{K}_T$ is obtained by taking into account the torsional restraint of the beam spring only. Thus,

$$\overline{K}_T = \frac{Et^3bd}{6(1+\mu)hD_2\pi l} \tag{3}$$

The lower-limit values are $\overline{K}_T = 0.005$ for panel I and $\overline{K}_T = 0.037$ for panel II.

The nondimensional theoretical natural frequencies are compared with experimentally obtained results in figure 9. The dashed curve in figure 9(a) is the theoretical frequency based on the calculated values of $\overline{K}_D$ and $\overline{K}_R$ given in equations (1) and (2) and the lower limit of $\overline{K}_T$. As can be seen, the theory does not agree with experiment. However, as shown by the solid curve, when $\overline{K}_T$ is arbitrarily increased to a value of 1.1, theory is brought into excellent agreement with experiment. Since a reliable calculated estimate of $\overline{K}_T$ is not available, the higher value of $\overline{K}_T$ shown in the figure is presumed to be the more realistic value and should be used in the flutter calculations. Thus the final support spring constants for panel I are $\overline{K}_D = 0.918$, $\overline{K}_R = 0.098$, and $\overline{K}_T = 1.1$.

The spring constants for panel II were determined with the aid of figure 9(b). As shown by the dashed curve, the use of the lower limit of $\overline{K}_T$ again resulted in poor agreement between theory and experiment. However, unlike panel I, no value of $\overline{K}_T$ could be found to produce satisfactory agreement of theory with experiment when the original calculated estimates of $\overline{K}_D$ and $\overline{K}_R$ were used, as shown by the dot-dash curve which corresponds to $\overline{K}_T = \infty$. Thus, in order to match the experimentally obtained natural frequencies, other values of $\overline{K}_D$ and/or $\overline{K}_R$ were required. An expression for determining new values of $\overline{K}_D$ and $\overline{K}_R$ was derived by considering the beam spring only. For a cantilever beam clamped at the root and elastically restrained and loaded at the tip, the deflectional stiffness is related to the rotational stiffness according to strength-of-materials theory by

$$\overline{K}_D = \frac{12\overline{E}}{\pi^3}\left(\frac{b}{l}\right)^3 \left(\frac{1}{\dfrac{3}{\dfrac{\overline{K}_R}{\overline{E}}\dfrac{l}{b}\pi} + 1} \right) \tag{4}$$

where $0 \leqq K_R \leqq \infty$.

The actual amount of rotation at the beam tip was not measured. However, by selecting values of $\overline{K}_R$, corresponding values of $\overline{K}_D$ were determined from equation (4). Then, for each combination of $\overline{K}_D$ and $\overline{K}_R$, various values of $\overline{K}_T$ were tried until the theory gave the best agreement with the measured natural frequencies. The best agreement for panel II $\left(\overline{K}_D = 7.1,\ \overline{K}_R = 2.5,\ \overline{K}_T = 8\right)$ is shown by the solid curve in figure 9(b). The final values of $\overline{K}_T$ for panels I and II are seen to be over two orders of magnitude higher than those values obtained from equation (3) for the beam only. Thus it would

appear that the primary torsional stiffness $\overline{K}_T$ results from the doubler strap. The selection of the final values of $\overline{K}_D$, $\overline{K}_R$, and $\overline{K}_T$ were based on the best agreement of theory with experiment; these values are given in table IV.

Flutter predictions for zero in-plane loading.- The selected (final) values of $\overline{K}_D$, $\overline{K}_R$, and $\overline{K}_T$ given in table IV were used to define the natural frequencies and corresponding natural mode shapes for the flutter analysis of appendix B. The variation of panel frequencies with dynamic-pressure parameter λ is shown in figures 10(a) and 10(b) for panels I and II, respectively. The behavior of only the first four modes is shown. As the dynamic pressure increases, modes two and three approach each other until they coalesce. At this point (the maximum point on the loop) the panel becomes unstable and flutter occurs for any increase in λ. The resulting flutter mode shapes, then, are defined predominantly by modes two and three. These theoretical flutter mode shapes are shown in figures 11(a) and 11(b) for panels I and II, respectively.

The critical flutter dynamic-pressure parameter predicted by theory for zero in-plane loading is $\lambda_{cr} = 11\ 235$ for panel I and $\lambda_{cr} = 59\ 700$ for panel II. These values of λ_{cr} are nearly a factor of 3 greater than the values obtained from the linear extrapolation of the experimental data in figure 6.

In light of the apparent discrepancy between theory and the extrapolated experimental flutter dynamic pressure q_{cr} of each test panel, the question arises about the sensitivity of q_{cr} to variations in panel support stiffnesses and panel bending and twisting stiffnesses. These quantities are not amenable to simple calculation for the complex panels tested, and the validity of the values used should be established.

The effect of $\overline{K}_T$ on the critical flutter dynamic pressure of panel I is shown in figure 12 where λ_{cr} is plotted against $\overline{K}_T$ from 0 to 1.0 and $1/\overline{K}_T$ from 1.0 to 0. The curve represents the critical flutter dynamic pressure over the entire range of $\overline{K}_T$. In previous investigations of corrugation-stiffened panels, $\overline{K}_T$ was assumed to be zero (for example, ref. 4), since measured natural frequencies were either unavailable or insufficient to evaluate the torsional boundary restraint properly. However, as can be seen, $\overline{K}_T$ has a major influence on λ_{cr} for panel I and is capable of increasing λ_{cr} from 435 for $\overline{K}_T = 0$ to 16 725 for $\overline{K}_T = \infty$. (The value of λ_{cr} for $\overline{K}_T = \infty$ is identical to the value for $\overline{K}_D = \infty$.) The symbol shown in figure 12 represents the extrapolated experimental result for panel I and is seen to be only 35 percent of the predicted value based on the values of spring constants given in table IV. However, if $\overline{K}_T$ is neglected (left-hand limit of curve), the predicted value of λ_{cr} is seen to be about an order of magnitude below experiment. It is apparent that if $\overline{K}_T$ were adjusted from 1.1 to 0.3, theory and experiment would be in agreement; however, this value of $\overline{K}_T$ resulted in theoretical

natural frequencies of the panels that differed considerably from those measured. Thus, large adjustments in $\overline{K}_T$ from the value shown by the symbol are considered to be unwarranted.

A study was also made of the effects of the panel bending stiffness D_1 and twisting stiffness D_{xy} on vibration and flutter characteristics of the panels. These stiffnesses are of major importance in classical panel flutter analysis but are often difficult to determine accurately for a fabricated corrugation-stiffened panel; any inaccuracies in their values could cause erroneous flutter results. The results of the study are given in table V.

Table V shows the effect of arbitrary 50-percent reductions in D_1 and D_{xy} on flutter dynamic pressure q_{cr}. In addition, changes in several of the panel natural frequencies are shown as a function of the "best agreement" theoretical natural frequencies. (See solid curves in fig. 9.) The reference values of D_1 and D_{xy} used in the table correspond to the calculated values given in table I. Table V shows that q_{cr} remains essentially unchanged for both panels when D_{xy} remains fixed and D_1 is reduced. Note that the natural frequencies, however, begin to show some disagreement (especially for panel I at the higher values of m) with values based on calculated panel stiffnesses and spring constants. (The reference frequencies have already been shown in figure 9 to be in good agreement with experiment.) Thus, the original calculated value $D_{1,ref}$ is adequate for the flutter analysis, since a 50-percent reduction in D_1 does not appreciably affect q_{cr}.

In contrast, when D_{xy} is reduced by a factor of 2 and D_1 remains fixed, a corresponding reduction in q_{cr} of approximately 50 percent is realized. Although this reduction in q_{cr} would bring theory and the extrapolated flutter point (for zero in-plane loading) into much better agreement, a check of the natural frequencies shows poor agreement with the reference values for both panels. Even when drastic changes in spring constants were explored, the reference frequencies could not be satisfactorily matched. It was therefore concluded from this study that it is impossible to predict both the extrapolated flutter points and the natural-vibration characteristics accurately for the test panels by using the same set of panel stiffness and support stiffnesses. Inasmuch as more confidence can be placed in the experimentally determined natural frequencies than the flutter points for zero in-plane loading (which are results of large extrapolations), the panel and support stiffnesses determined from the vibration analysis are probably reasonably accurate.

Flutter predictions for uniform in-plane loading.- Some insight into the discrepancy between theory and the extrapolated experimental flutter point may be found by examining the theory for panels subjected to uniform in-plane loading. The theoretical flutter boundaries for the two panels of this investigation are shown in figures 13(a) and 13(b)

in which the cube root of the critical dynamic-pressure parameter is plotted against the ratio of uniform in-plane loading in the streamwise direction N_x to the buckling load $N_{x,cr}$. The theoretical boundaries determined from the analysis in appendix B are shown by the solid curves for the cross-stream in-plane load $N_y = 0$. Although the panel has a temperature variation through the depth of the corrugations, which sets up a self-equilibrating thermal stress system, this stress is neglected in the theory. The experimental data obtained from figures 6(a) and 6(b) are shown by the symbols. The data are plotted by using assumed critical buckling temperature changes near the highest temperature at which flutter was initiated. The values are 230° F (128 K) for panel I and 80° F (44 K) for panel II. Furthermore, it was assumed that in-plane load N_x varied directly with temperature. Although the experimental data are bracketed by the theoretical values of λ_{cr} at $N_x = 0$ and λ_{cr} at buckling $\left(N_x/N_{x,cr} = 1\right)$, it is apparent that the data do not follow the trend of the theoretical flutter boundaries, especially in the region near buckling. It is also apparent that linear extrapolation of the data to zero N_x may lead to large discrepancies.

The zero values of the flutter parameter predicted by theory at loads smaller than the critical buckling load are characteristic of long, narrow isotropic panels subjected to uniform in-plane loads when structural damping is neglected. (See ref. 9.) In fact, on an analytical basis, long, narrow isotropic panels are equivalent to short orthotropic panels oriented in the airstream as in this investigation. A recent investigation presented in reference 10 has indicated that for long, narrow isotropic panels, structural and aerodynamic damping can significantly increase λ_{cr} in the region near buckling. This increase is illustrated in figure 14, where the cube root of λ_{cr} is plotted against the uniform in-plane loading ratio for an isotropic panel with length-to-width ratio of 10. Experimental flutter data presented in reference 11 for a similar panel are also shown in the figure. The theory assumes clamped-edge boundary conditions. The flutter boundary obtained with no damping is similar to the boundaries of figure 13 and does not follow the experimental trend for values of $N_x/N_{x,cr} > 0.5$. However, with structural and aerodynamic damping included, the trend near buckling is changed dramatically; whereas for $N_x/N_{x,cr} < 0.5$, damping has negligible effect on λ_{cr}. Thus, reference 10 indicates that when structural damping is included in the theory for isotropic panels, the flutter predictions near buckling are greatly improved and the theoretical boundary more closely follows the experimental trend.

The influence of structural damping on flutter of spring-supported orthotropic panels is beyond the scope of this paper. However, the salient fact is that the amount of experimental data obtained for the two panels of this investigation is insufficient for linear extrapolation of the data as shown in figure 6 to accurately predict flutter dynamic pressure for $N_x = 0$. In fact, in light of the theoretical boundary for stressed panels, it is

believed that structural damping would have to be included in the theory to make a meaningful comparison with experiment.

CONCLUDING REMARKS

Natural-vibration and flutter characteristics of two corrugation-stiffened panels with elastically restrained edges were studied both experimentally and analytically. The analysis, which uses small-deflection theory and piston-theory aerodynamics, accounts for finite deflectional, rotational, and torsional stiffnesses of the boundary supports and uniform in-plane loading. Flutter tests were made for the panels subjected to airflow at a Mach number of 3. The panel edges normal to the corrugations (streamwise edges) were supported on cantilever beam springs. The support torsional stiffness resulted primarily from corrugated doubler straps welded to the panel at the ends of the corrugations. Panel leading and trailing edges were essentially simply supported.

The natural-vibration data for the two test panels exhibit excellent agreement with theory when the finite deflectional, rotational, and torsional stiffnesses of the boundary supports are taken into account in the theory. Only one set of support spring constants that permitted correlation between theory and experiment could be found for each test specimen. Furthermore, the theory shows that for panels on flexible supports, the addition of torsional stiffening at the supports is a definite asset for increasing flutter dynamic pressure. This method of support torsional stiffening may be a means for increasing flutter resistance of panels for which the supports are designed to permit thermal expansion.

The experimental flutter boundaries obtained as a function of uniform in-plane loading exhibit fair agreement with theory at moderate loading levels. Linear extrapolation of the data to zero uniform in-plane loading resulted in experimental flutter dynamic pressures considerably lower than the theoretical predictions. At in-plane loading levels near buckling, however, the experimental critical dynamic pressures were much greater than theoretical predictions. Examination of theoretical results for the test panels subjected to uniform in-plane loading indicated that flutter behavior was similar to that of panels for which structural damping has been shown to have a pronounced effect at loading levels near buckling. It is believed that structural and aerodynamic damping must also be included in the theory for flutter of orthotropic panels subjected to uniform in-plane loading before a meaningful comparison of theory and experiment can be made.

Langley Research Center,
National Aeronautics and Space Administration,
Hampton, Va., August 3, 1970.

APPENDIX A

CONVERSION OF U.S. CUSTOMARY UNITS TO SI UNITS

The International System of Units (SI) was adopted by the Eleventh General Conference on Weights and Measures, Paris, October 1960. (See ref. 5.) Conversion factors for the units used herein are given in the following table:

Physical quantity	U.S. Customary Unit	Conversion factor (*)	SI Unit (**)
Length	in.	0.0254	meters (m)
Pressure	lbf/ft^2	47.88	newtons/$meter^2$ (N/m^2)
Stiffness	lbf-in.	0.113	newton-meter (N-m)
Strength	lbf/in^2	6.895×10^3	newtons/$meter^2$ (N/m^2)
Temperature . .	^oF	(5/9)(F + 459.67)	kelvins (K)

*Multiply value given in U.S. Customary Unit by conversion factor to obtain equivalent value in SI Unit.

**Prefixes to indicate multiples of units are as follows:

Prefix	Multiple
kilo (k)	10^3
centi (c)	10^{-2}
milli (m)	10^{-3}

APPENDIX B

FLUTTER ANALYSIS OF PANELS ON ELASTIC SUPPORTS

Flutter Solution

The orthotropic panel and the coordinate system are shown in figure 7. The leading and trailing edges ($x = 0$ and $x = a$, respectively) are simply supported; the spanwise edges $\left(y = \pm\frac{b}{2}\right)$ are supported by deflectional, rotational, and torsional springs. The spring constants per unit length are K_D, K_R, and K_T corresponding to deflection, rotation, and torsion. The panel is loaded by uniform in-plane loads N_x and N_y. Airflow at Mach number M passes over one surface of the panel in the x-direction (normal to the corrugations). The aerodynamic loading is given by the two-dimensional static approximation.

The present analysis closely parallels the model analysis presented in appendix B of reference 3. However, in reference 3 only deflectional springs were considered, and the effect of in-plane load was not included. With the addition of the in-plane load terms, the governing differential equation given in reference 3 becomes

$$D_1 \frac{\partial^4 w}{\partial x^4} + 2D_{12} \frac{\partial^4 w}{\partial x^2 \partial y^2} + D_2 \frac{\partial^4 w}{\partial y^4} + N_x \frac{\partial^2 w}{\partial x^2} + N_y \frac{\partial^2 w}{\partial y^2} + 2 \frac{\partial^2 w}{\partial \tau^2} + \frac{2q}{\sqrt{M^2 - 1}} \frac{\partial w}{\partial x} = 0 \tag{B1}$$

where

$$D_1 = \frac{D_x}{1 - \mu_x \mu_y}$$

$$D_2 = \frac{D_y}{1 - \mu_x \mu_y}$$

$$D_{12} = D_{xy} + \mu_x D_2$$

The boundary conditions at the leading and trailing edges, that is, simple supports, are

$$w(0,y,\tau) = w(a,y,\tau) = \frac{\partial^2 w}{\partial x^2}(0,y,\tau) = \frac{\partial^2 w}{\partial x^2}(a,y,\tau) = 0 \tag{B2}$$

At the spring-supported (streamwise) edges, the boundary conditions to be satisfied can be obtained from appendix C of reference 12. The results are

$$\left.\begin{aligned}&\left[D_2\left(\frac{\partial^2 w}{\partial y^2} + \mu_x \frac{\partial^2 w}{\partial x^2}\right) \pm K_R \frac{\partial w}{\partial y}\right]_{y=\pm\frac{b}{2}} = 0 \\ &\left[\pm K_D w \mp K_T \frac{\partial^2 w}{\partial x^2} - \left(D_{12} + D_{xy}\right) \frac{\partial^3 w}{\partial x^2 \partial y} - D_2 \frac{\partial^3 w}{\partial y^3} - N_y \frac{\partial w}{\partial y}\right]_{y=\pm\frac{b}{2}} = 0\end{aligned}\right\} \quad \text{(B3)}$$

The Galerkin procedure is employed to obtain solutions of equation (B1). A solution is assumed to be of the form

$$w = \sum_{m=1}^{\infty} A_m Y_m\left(\frac{y}{b}\right) \sin \frac{m\pi x}{a} e^{i\omega\tau} \quad \text{(B4)}$$

where $Y_m\left(\frac{y}{b}\right)$ is the fundamental cross-stream panel mode shape for no airflow and is dependent on m, since the side edges can deflect. By following the procedure of reference 3, equation (B4), which satisfies equation (B2), is then substituted into equation (B1). The resulting equation is multiplied by $Y_n\left(\frac{y}{b}\right) \sin\left(\frac{n\pi x}{a}\right)$ and is integrated over the area to obtain the following set of simultaneous equations:

$$\left[\left(\frac{\omega_m}{\omega_r}\right)^2 - \left(\frac{\omega}{\omega_r}\right)^2\right] A_m + \frac{\lambda}{\pi^4} \sum_{n=1}^{j} \left[1 - (-1)^{m+n}\right] \frac{2mn}{(n^2 - m^2)} \frac{C_{m,n}}{C_{m,m}} A_n = 0 \quad \text{(B5)}$$

where $m = 1, 2, 3, \ldots, j$; $n \neq m$; and

$$C_{m,n} = \int_{-1/2}^{1/2} Y_m\left(\frac{y}{b}\right) Y_n\left(\frac{y}{b}\right) d\left(\frac{y}{b}\right) \quad \text{(B6)}$$

The determinant of the coefficients of A_m (eq. (B5)) is the flutter determinant which must vanish for nontrivial solutions to exist. The frequency ω is taken as the eigenvalue.

Natural Mode Shapes

The cross-stream natural mode shapes Y_m must be such that boundary conditions (eqs. (B3)) are satisfied. A suitable set of Y_m can be obtained by solving the corresponding natural vibration problem This solution can be accomplished by substituting equation (B4) into equation (B1) with the aerodynamic loading term set equal to zero. This procedure yields the following differential equation for each Y_m:

$$Y_m'''' + \pi^2 \overline{A}_{y,m} Y_m'' - \pi^4 \overline{B}_{y,m} Y_m = 0 \tag{B7}$$

where

$$\overline{B}_{y,m} = \left(\frac{b}{a}\right)^4 \frac{D_1}{D_2}\left[\left(\frac{\omega_m}{\omega_r}\right)^2 + m^2\left(\frac{N_x a^2}{\pi^2 D_1} - m^2\right)\right] \tag{B8}$$

and

$$\overline{A}_{y,m} = \frac{N_y b^2}{\pi^2 D_2} - 2\left(\frac{mb}{a}\right)^2 \frac{D_{12}}{D_2} \tag{B9}$$

The solution of equation (B7) can be written as

$$Y_m = C_m \cosh \frac{\epsilon y}{b} + D_m \cos \frac{\delta y}{b} \tag{B10}$$

where

$$\left.\begin{aligned} \epsilon &= \pi\sqrt{-\frac{\overline{A}_{y,m}}{2} + \sqrt{\frac{\overline{A}_{y,m}}{4} + \overline{B}_{y,m}}} \\ \delta &= \pi\sqrt{\frac{\overline{A}_{y,m}}{2} + \sqrt{\frac{\overline{A}_{y,m}}{4} + \overline{B}_{y,m}}} \end{aligned}\right\} \tag{B11}$$

Equations (B4) and (B10) are substituted into the boundary conditions (eqs. (B3)) in order to obtain two simultaneous equations in terms of the coefficients C_m and D_m. By setting the determinant of these coefficients equal to zero, a transcendental equation is obtained which, when satisfied, insures that the boundary conditions are also satisfied. The resulting transcendental equation (for $\mu_x = 0$) is

$$\begin{aligned} &\epsilon\delta^4 \cos\frac{\delta}{2}\tanh\frac{\epsilon}{2} + \delta\epsilon^4 \sin\frac{\delta}{2} - \pi^3\left\{\left[\overline{K}_D + \overline{K}_T\left(\frac{mb}{a}\right)^2\right]\cos\frac{\delta}{2}\right. \\ &\left. - \frac{\epsilon\delta}{\pi^2}\overline{K}_R \sin\frac{\delta}{2}\tanh\frac{\epsilon}{2}\right\}(\epsilon^2 + \delta^2) \\ &- \pi^4\overline{K}_R\left[\overline{K}_D + \overline{K}_T\left(\frac{mb}{a}\right)^2\right]\left(\delta \sin\frac{\delta}{2} + \epsilon \cos\frac{\delta}{2}\tanh\frac{\epsilon}{2}\right) = 0 \end{aligned} \tag{B12}$$

where

$$\left.\begin{aligned} \overline{K}_D &= \frac{K_D}{D_2}\left(\frac{b}{\pi}\right)^3 \\ \overline{K}_R &= \frac{K_R b}{D_2 \pi} \\ \overline{K}_T &= \frac{K_T b}{D_2 \pi} \end{aligned}\right\} \tag{B13}$$

The expression for the natural mode shape Y_m given in equation (B10) can be rewritten as

$$\frac{Y_m}{C_m} = \cosh \frac{\epsilon y}{b} + \frac{D_m}{C_m} \cos \frac{\delta y}{b} \tag{B14}$$

where

$$\frac{D_m}{C_m} = \frac{\delta^2 \cos \frac{\delta}{2} + \pi \overline{K}_R \delta \sin \frac{\delta}{2}}{\epsilon^2 \cosh \frac{\epsilon}{2} + \pi \overline{K}_R \epsilon \sinh \frac{\epsilon}{2}} \tag{B15}$$

An examination of equation (B12) reveals the beneficial effect of large $\overline{K}_T$ on panel flutter dynamic pressure. The sum of the $\overline{K}_D$ and $\overline{K}_T\left(\frac{mb}{a}\right)^2$ terms can be thought of as an effective spring stiffness term which controls panel flutter dynamic pressure. Thus, if the value of $\overline{K}_T$ can be made large enough, the flutter dynamic pressure of a simply supported panel can be approached regardless of how small the value of $\overline{K}_D$ may be. It should also be noted that $\overline{K}_T$ becomes more effective with increasing m.

Equations (B6), (B8), (B9), (B11), (B12), (B14), and (B15) are used to determine the elements of the flutter determinant in the following manner:

1. For a given panel, D_1, D_2, D_{12}, N_x, N_y, and a/b are specified; thus $\overline{A}_{y,m}$ (eq. (B9)) is known.

2. An iteration procedure is used to solve for $\overline{B}_{y,m}$ (eq. (B8)) to determine the values of ϵ and δ which satisfy equations (B11) and (B12) simultaneously. The solution values of ϵ and δ determine the cross-stream mode shape (eqs. (B14) and (B15)), which is used to evaluate $C_{m,n}$ (eq. (B6)). When these steps are completed, the elements of the flutter determinant are known, and the flutter behavior of the panel under consideration can be determined.

REFERENCES

1. Bohon, Herman L.; Anderson, Melvin S.; and Heard, Walter L., Jr.: Flutter Design of Stiffened-Skin Panels for Hypersonic Aircraft. NASA TN D-5555, 1969.

2. Bohon, Herman L.: Experimental Flutter Results for Corrugation-Stiffened Panels at a Mach Number of 3. NASA TN D-2293, 1964.

3. Bohon, Herman L.; and Anderson, Melvin S.: Role of Boundary Conditions on Flutter of Orthotropic Panels. AIAA J., vol. 4, no. 7, July 1966, pp. 1241-1248.

4. Bohon, Herman L.: Flutter of Corrugation-Stiffened Panels at Mach 3 and Comparison With Theory. NASA TN D-4321, 1968.

5. Comm. on Metric Pract.: ASTM Metric Practice Guide. NBS Handbook 102, U.S. Dep. Com., Mar. 10, 1967.

6. Stroud, W. Jefferson: Elastic Constants for Bending and Twisting of Corrugation-Stiffened Panels. NASA TR R-166, 1963.

7. Schaefer, William T., Jr.: Characteristics of Major Active Wind Tunnels at the Langley Research Center. NASA TM X-1130, 1965.

8. Herr, Robert W.; and Carden, Huey D.: Support Systems and Excitation Techniques for Dynamic Models of Space Vehicle Structures. Proceedings of Symposium on Aeroelastic & Dynamic Modeling Technology, RTD-TDR-63-4197, Pt. I, U.S. Air Force, Mar. 1964, pp. 249-277.

9. Dixon, Sidney C.: Comparison of Panel Flutter Results From Approximate Aerodynamic Theory With Results From Exact Inviscid Theory and Experiment. NASA TN D-3649, 1966.

10. Shore, Charles P.: Effects of Structural Damping on Flutter of Stressed Panels. NASA TN D-4990, 1969.

11. Dixon, Sidney C.; Griffith, George E.; and Bohon, Herman L.: Experimental Investigation at Mach Number 3.0 of the Effects of Thermal Stress and Buckling on the Flutter of Four-Bay Aluminum Alloy Panels With Length-Width Ratios of 10. NASA TN D-921, 1961.

12. Libove, Charles; and Batdorf, S. B.: A General Small-Deflection Theory for Flat Sandwich Plates. NACA Rep. 899, 1948. (Supersedes NACA TN 1526.)

TABLE I.- PANEL BENDING AND TWISTING STIFFNESS PARAMETERS

[Calculated by using method of ref. 6]

D_1	7.508 lbf-in. (0.848 N-m)
D_2	6484 lbf-in. (732.7 N-m)
D_{xy}	1342 lbf-in. (151.6 N-m)

TABLE II.- AVERAGE NATURAL FREQUENCIES

m	Panel I		Panel II	
	Average frequency, Hz	Deviation, Hz	Average frequency, Hz	Deviation, Hz
1	97	±2	127	±2
2	194	±2	154	±2
3	290	±4	195	±2
4	405	±2	238	±5
5	494	±4	294	±10
6	631	±1	345	±4
7	752	±1	397	±9
8	---	--	454	±5

TABLE III.- DATA FOR PANEL FLUTTER TESTS

Panel	Test	Total temperature		Start of flutter					End of flutter				
				q_{cr}		ΔT		f, Hz	q_{cr}		ΔT		f, Hz
		°F	K	$\frac{lbf}{ft^2}$	$\frac{kN}{m^2}$	°F	K		$\frac{lbf}{ft^2}$	$\frac{kN}{m^2}$	°F	K	
I	1	318	432	4931	236	133	74	205	4064	195	135	75	205
				4729	226	126	70	205	4307	206	110	61	205
	2	408	482	4589	220	158	88	205	3823	183	194	108	205
				4000	192	198	110	205	3432	164	197	109	205
	3	452	506	4933	236	162	90	195	4094	196	213	118	200
				3960	190	226	126	200					
	[a]4	360	455										
II	1	308	426	2975	142	58	32	180					
	2	303	424	2470	118	86	48	180					
	3	304	424	3230	155	36	20	255	2440	117	136	76	250
	4	399	477	2731	131	82	46	185					

[a]No flutter observed.

TABLE IV.- PANEL SUPPORT SPRING CONSTANTS

Panel	$\bar{K}_D$	$\bar{K}_R$	$\bar{K}_T$
I	0.918	0.098	1.1
II	7.1	2.5	8

TABLE V.- INFLUENCE OF PANEL BENDING STIFFNESS D_1 AND TWISTING STIFFNESS D_{xy} ON VIBRATION AND FLUTTER BEHAVIOR

Panel	$\frac{D_1}{D_{1,ref}}$ (a)	$\frac{D_{xy}}{D_{xy,ref}}$ (a)	q_{cr} lbf/in^2	q_{cr} kN/m^2	$\frac{\omega_m}{\omega_{m,ref}}$ (b) m = 1	m = 3	m = 5
I	1	1	119.3	822.6	1.0	1.0	1.0
	1/2	1	125.7	866.7	1.0	.97	.92
	1	1/2	68.7	474	.90	.83	.86
II	1	1	79.3	547	1.0	1.0	1.0
	1/2	1	80.0	552	1.0	.99	.96
	1	1/2	37.6	259	.97	.80	.79

[a] $D_{1,ref}$ and $D_{xy,ref}$ values are given in table I.

[b] Theoretical frequencies $\omega_{m,ref}$ based on $D_{1,ref}$ and $D_{xy,ref}$.

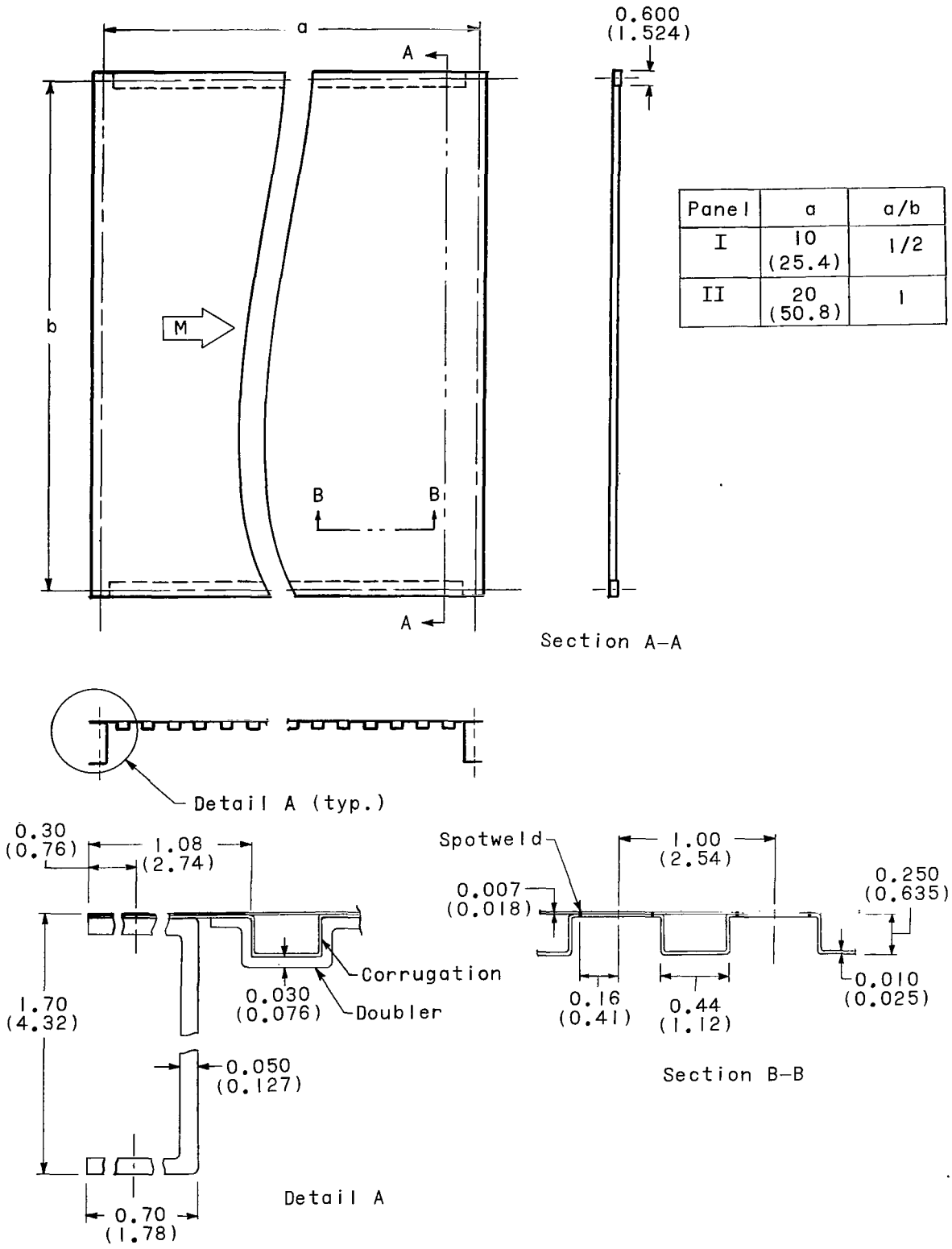

Panel	a	a/b
I	10 (25.4)	1/2
II	20 (50.8)	1

Figure 1.- Panel construction details. All dimensions are in inches (cm).

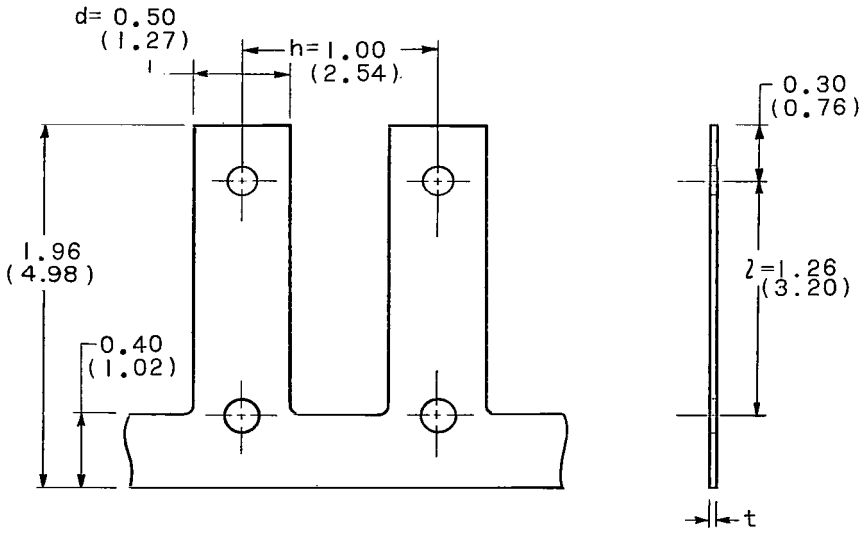

Panel	t
I	0.015 (0.038)
II	0.029 (0.074)

(a) Beam spring.

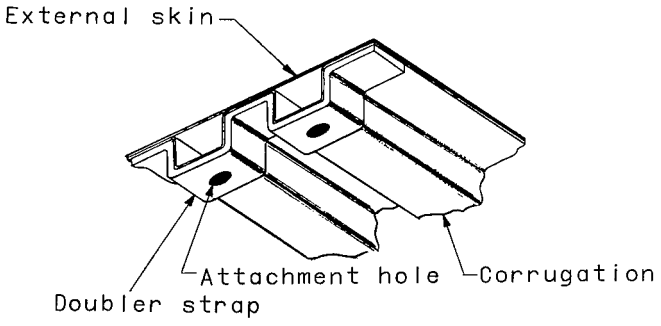

(b) Streamwise edge.

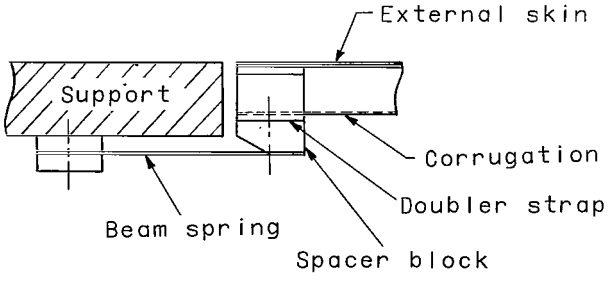

(c) Streamwise edge support.

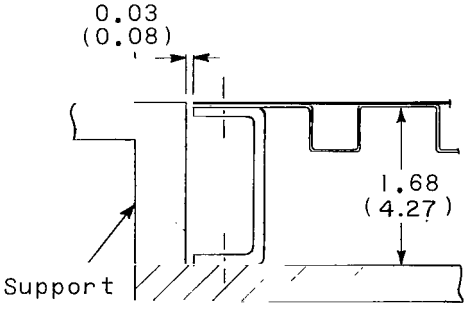

(d) Leading- and trailing-edge supports.

Figure 2.- Details of support springs and mounting arrangement. All dimensions are in inches (cm).

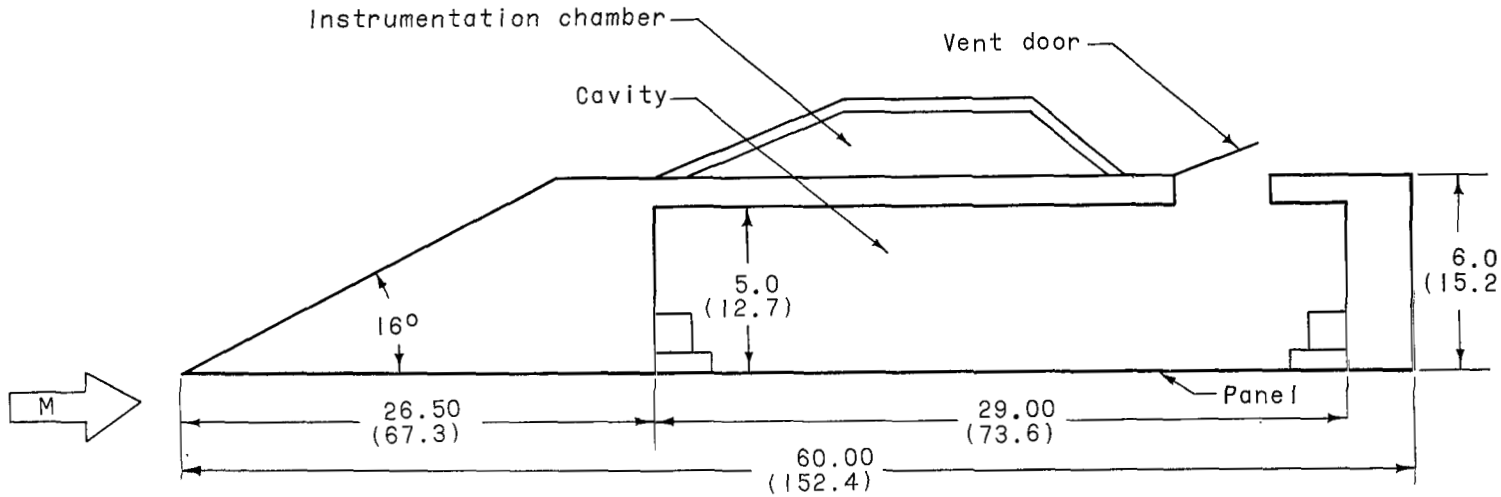

Figure 3.- Cross section of panel holder. All dimensions are in inches (cm).

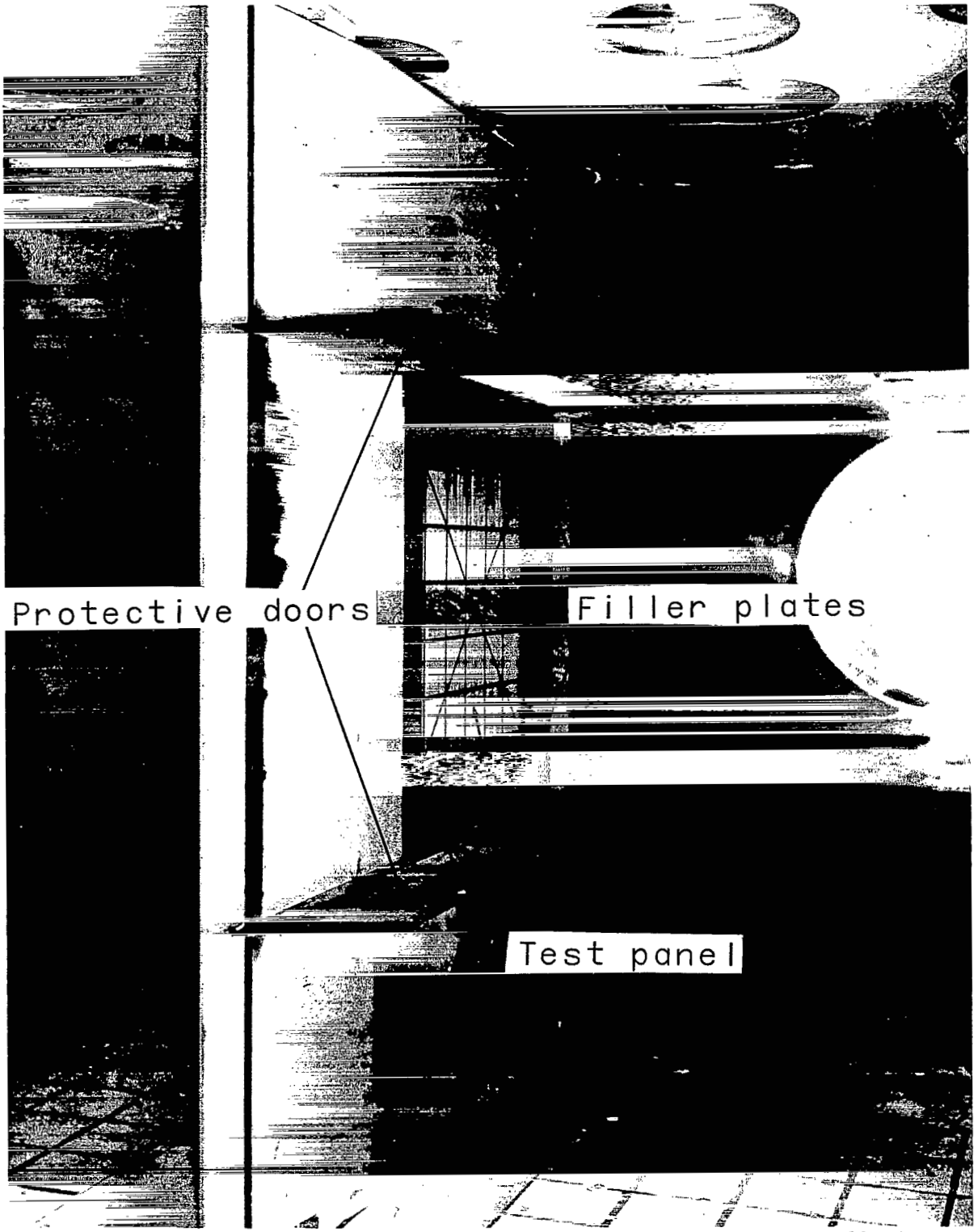

Figure 4.- View from upstream of test section showing panel holder with panel installed.

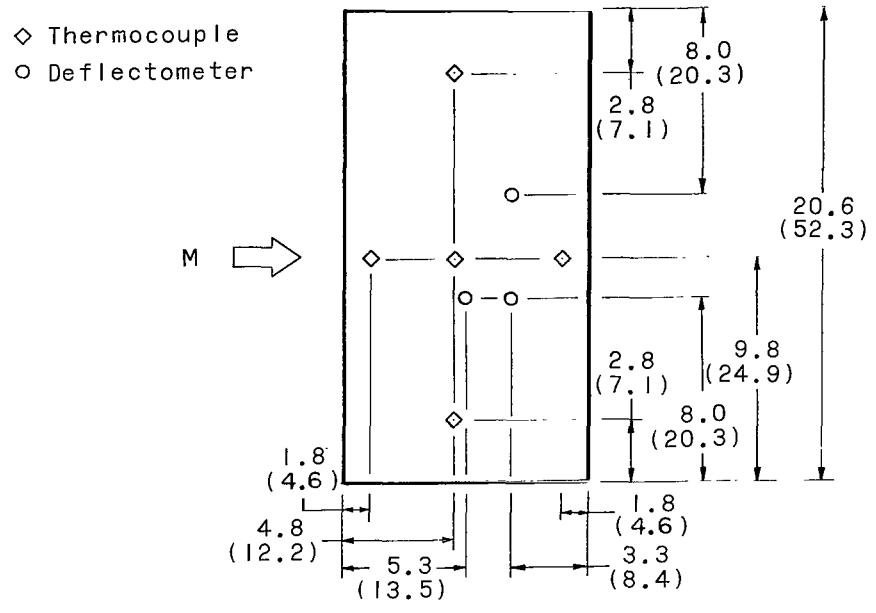

(a) Panel I.

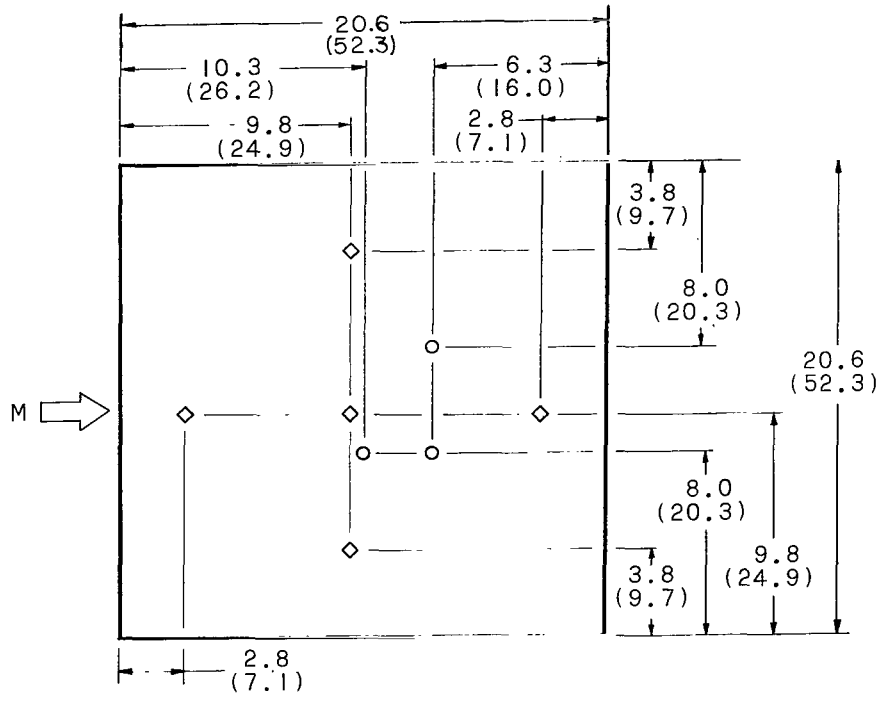

(b) Panel II.

Figure 5.- Panel instrumentation.
All dimensions are in inches (cm).

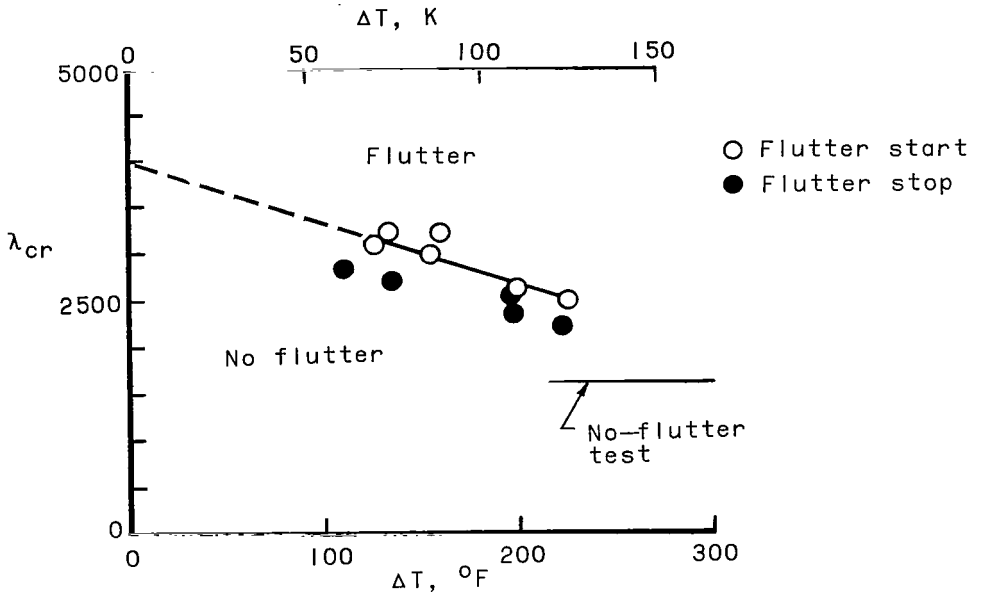

(a) Panel I.

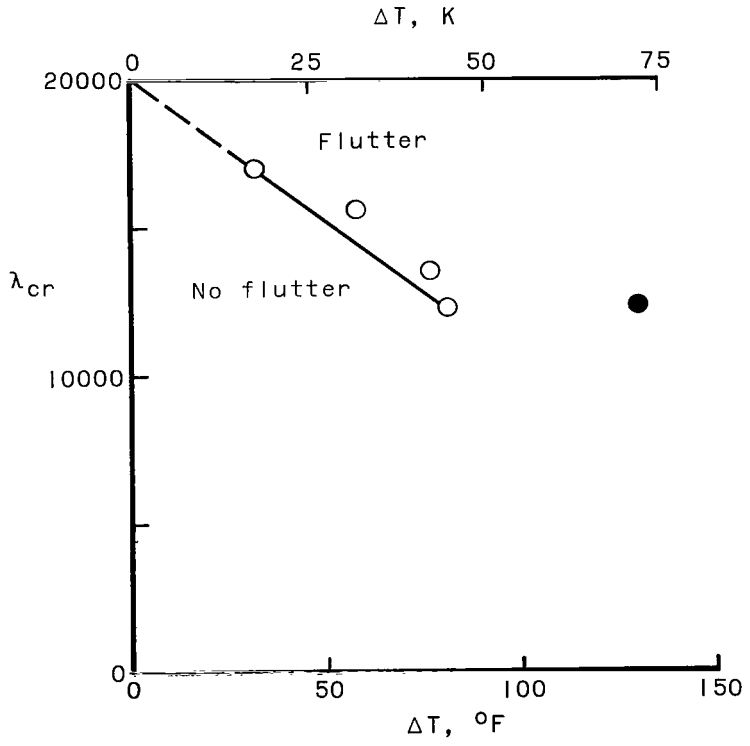

(b) Panel II.

Figure 6.- Experimental flutter data.

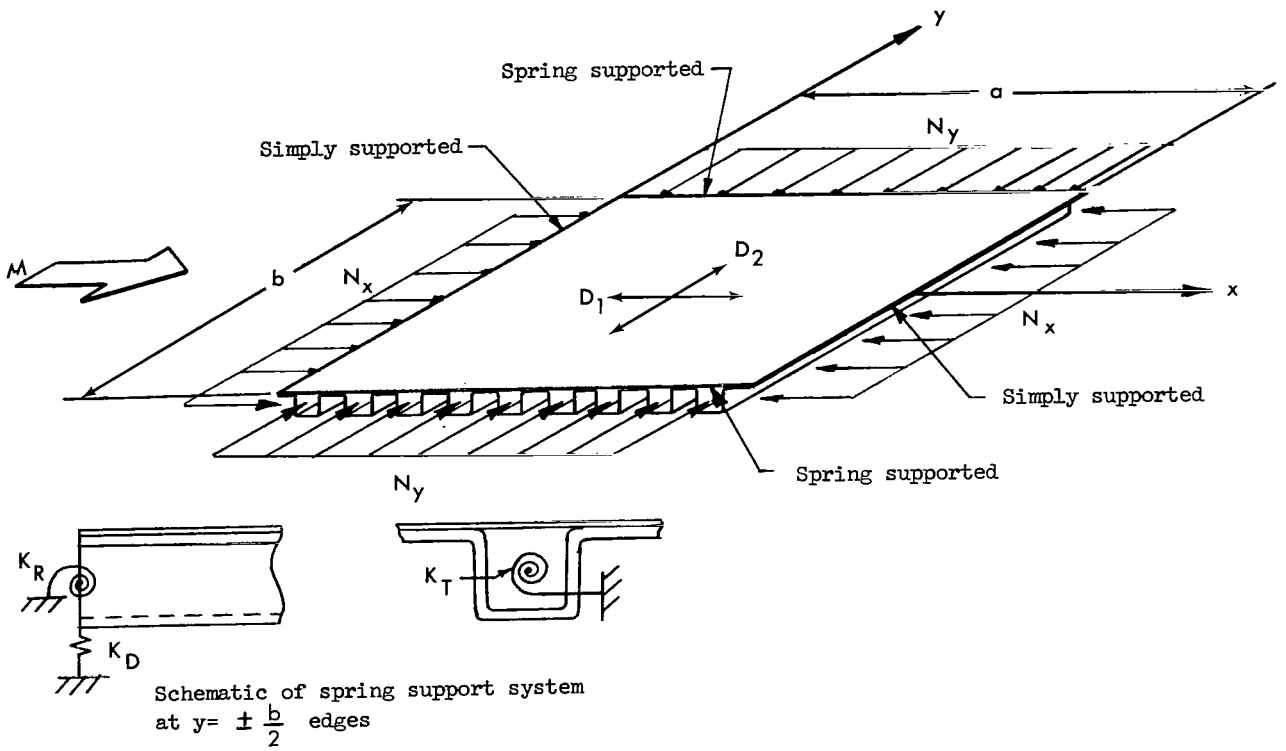

Figure 7.- Orthotropic panel and coordinate system and spring support system.

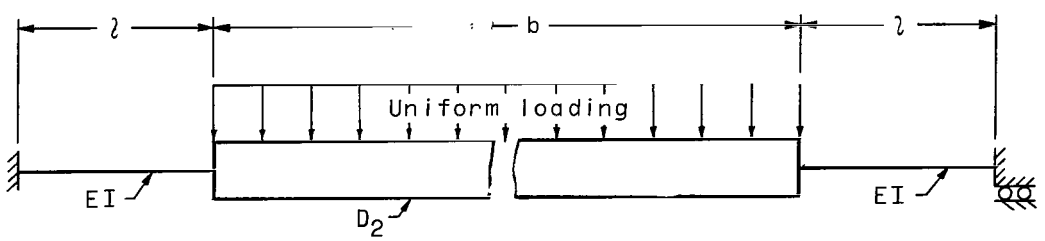

Figure 8.- Idealized structure for determining deflectional and rotational spring constants.

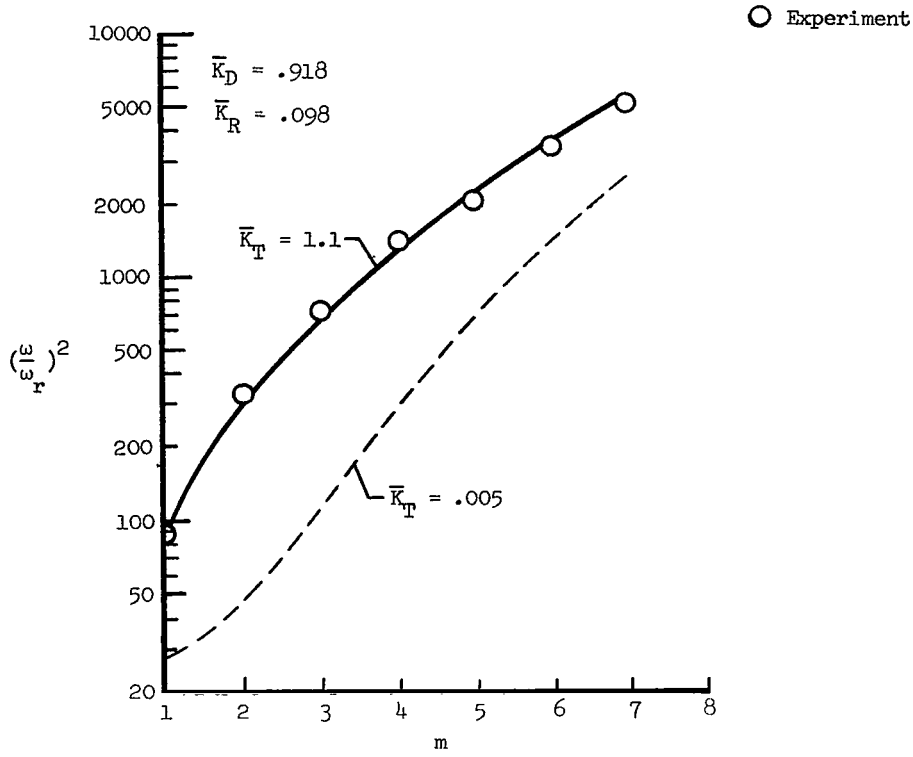

(a) Panel I; ω_r = 66.1 rad/s.

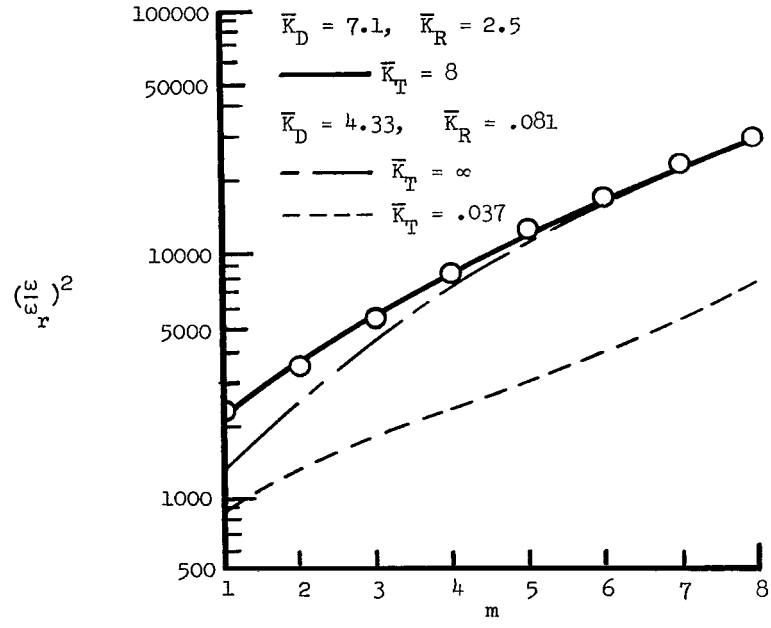

(b) Panel II; ω_r = 16.5 rad/s.

Figure 9.- Comparison of experimental natural frequencies with theory.

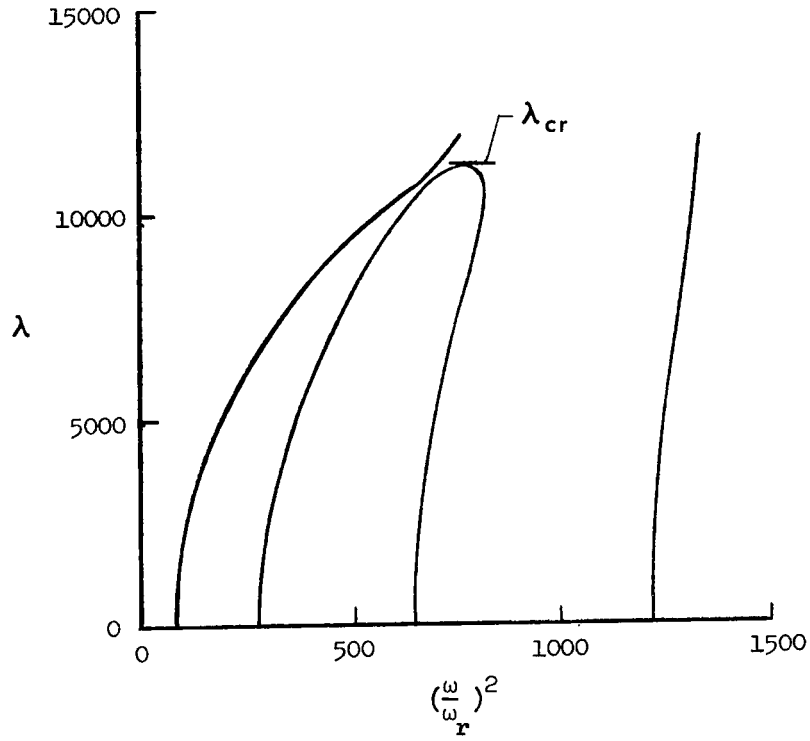

(a) Panel I (a/b = 1/2).

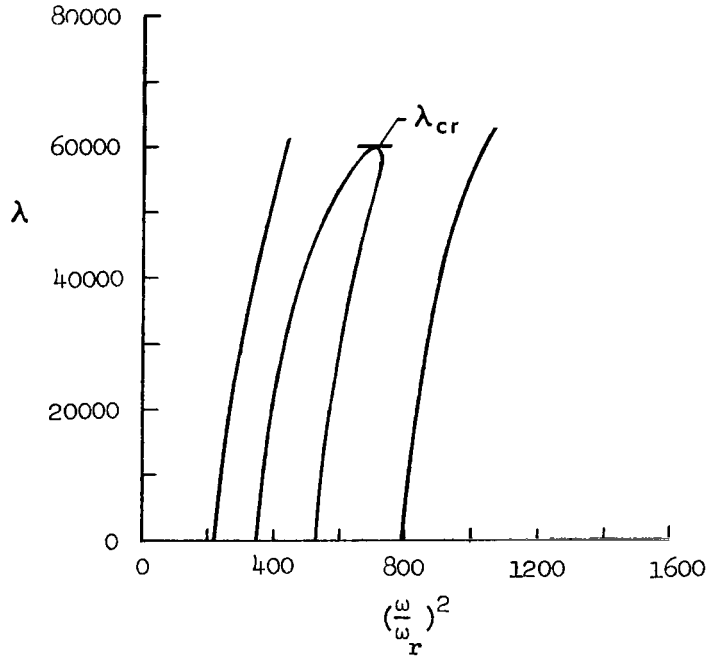

(b) Panel II (a/b = 1).

Figure 10.- Theoretical variation of four lowest natural panel frequencies with λ for zero uniform in-plane loading.

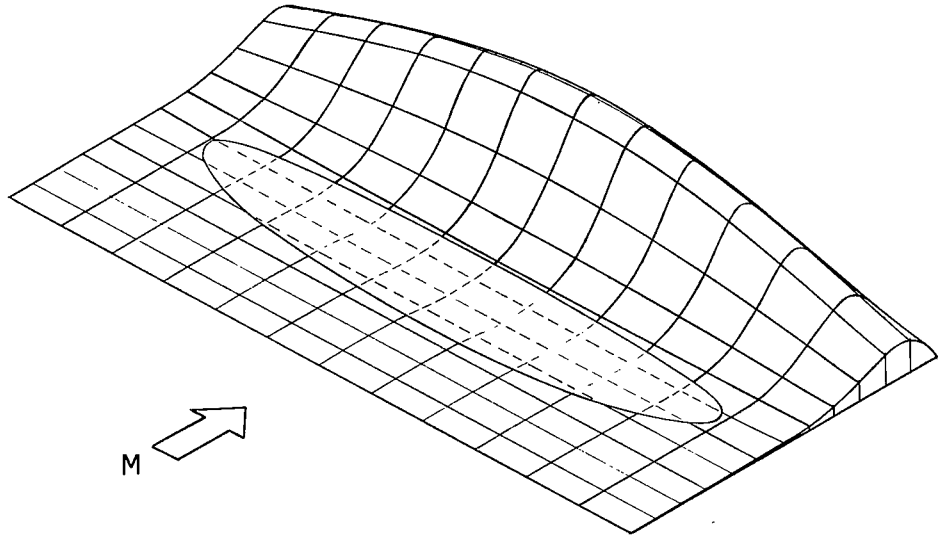

(a) Panel I.

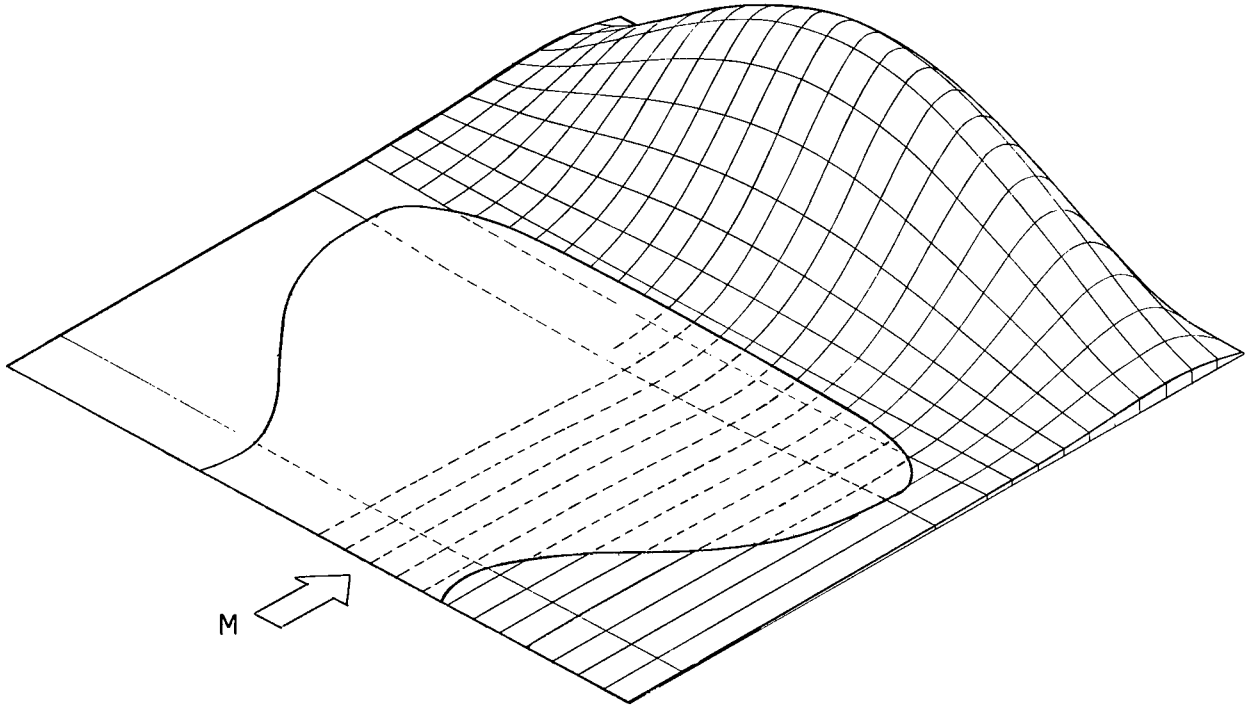

(b) Panel II.

Figure 11.- Theoretical flutter mode shapes for panels with zero uniform in-plane loading.

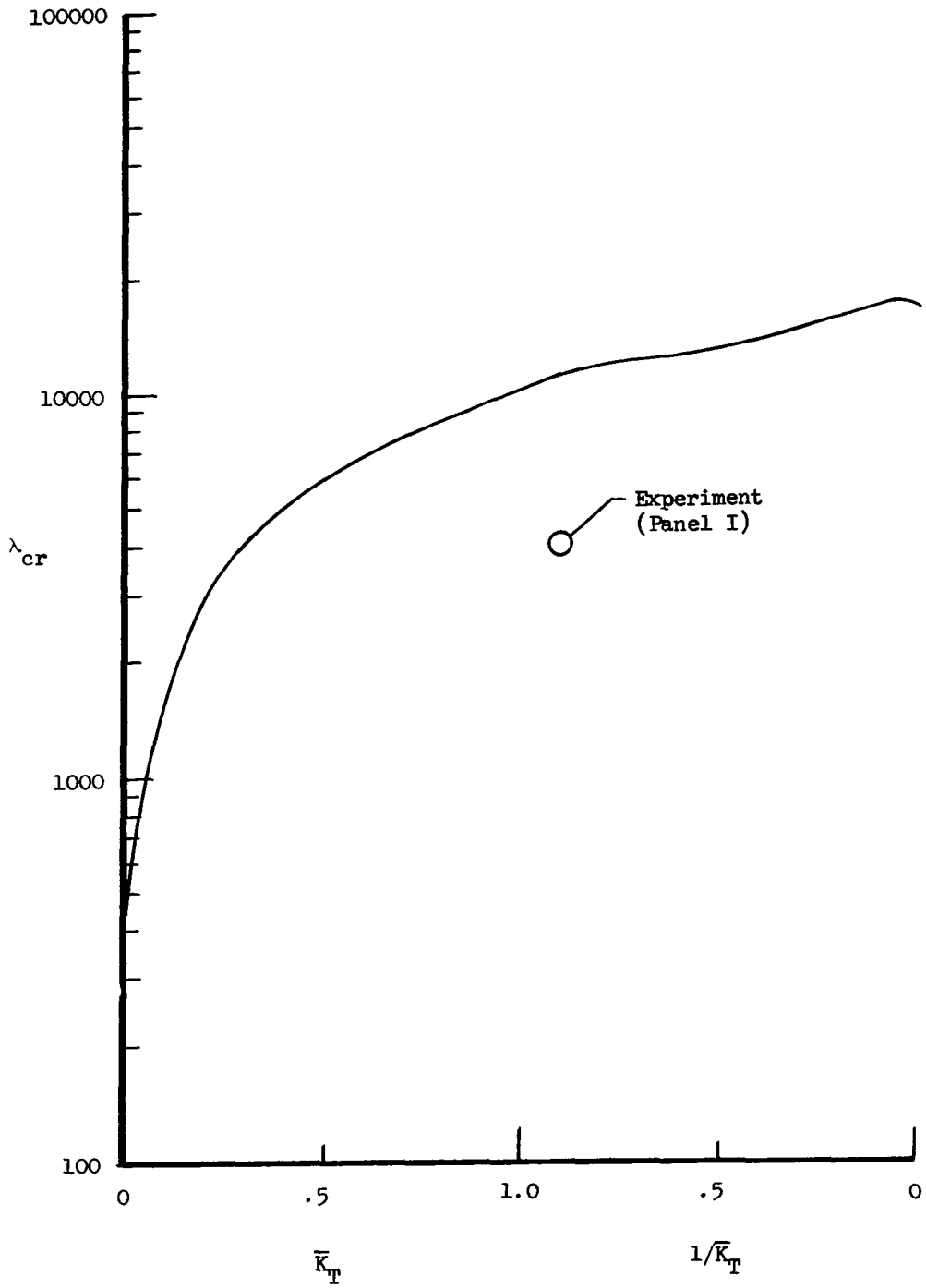

Figure 12.- Theoretical effect of torsional restraint on flutter dynamic pressure of panel I. $N_x = N_y = 0$; $\bar{K}_D = 0.918$; $\bar{K}_R = 0.098$.

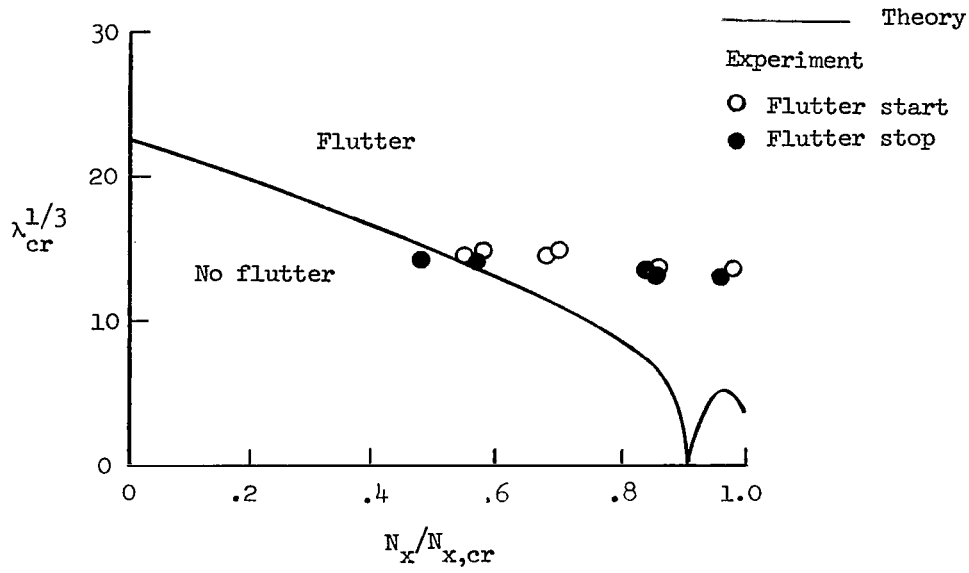

(a) Panel I (a/b = 1/2).

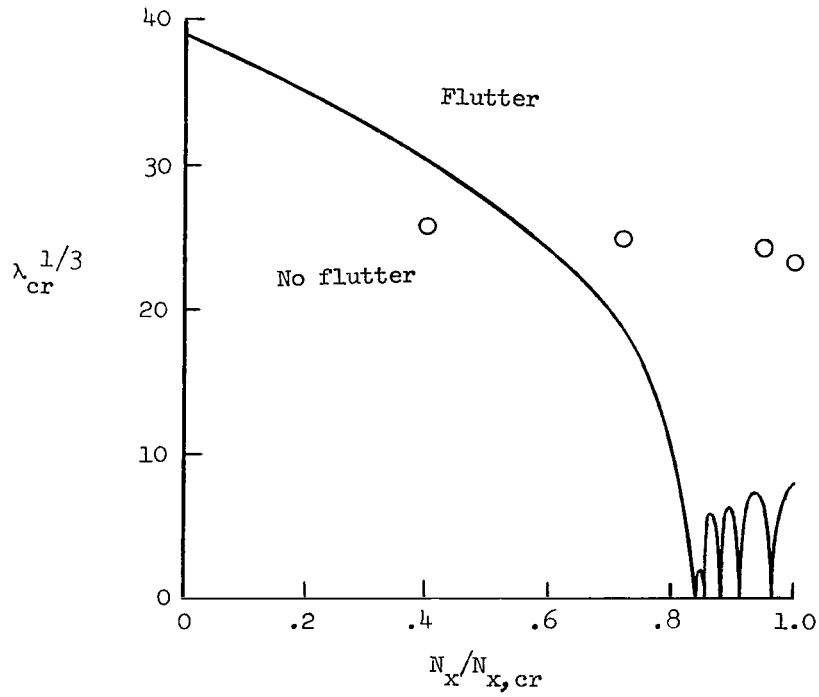

(b) Panel II (a/b = 1).

Figure 13.- Comparison of experiment with theoretical flutter boundaries for panels subjected to uniform in-plane loading. $N_y = 0$.

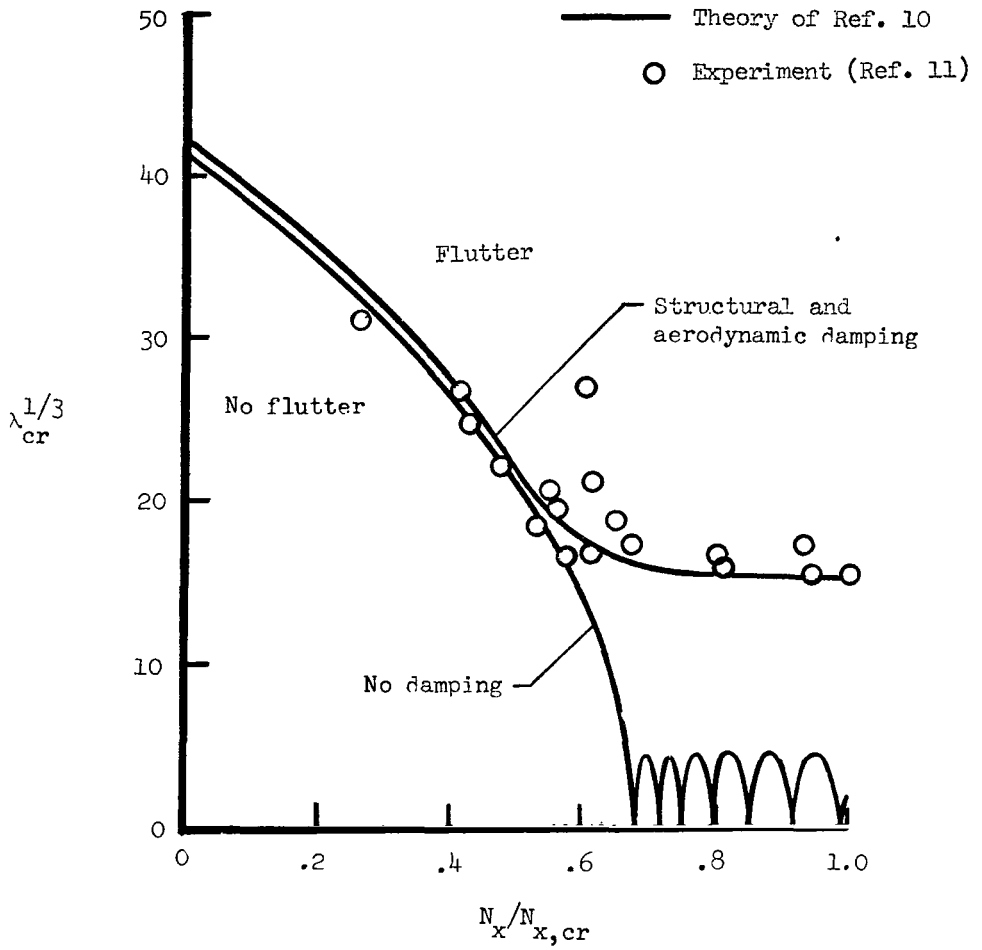

Figure 14.- Flutter boundaries for isotropic panel with clamped edges. a/b = 10.

NASA-Langley, 1970 —— 32 L-6772

06U 001 57 51 3DS 70272 00903
AIR FORCE WEAPONS LABORATORY /WLOL/
KIRTLAND AFB, NEW MEXICO 87117

ATT E. LOU BOWMAN, CHIEF,TECH. LIBRARY

"The aeronautical and space activities of the United States shall be conducted so as to contribute . . . to the expansion of human knowledge of phenomena in the atmosphere and space. The Administration shall provide for the widest practicable and appropriate dissemination of information concerning its activities and the results thereof."

—NATIONAL AERONAUTICS AND SPACE ACT OF 1958

NASA SCIENTIFIC AND TECHNICAL PUBLICATIONS

TECHNICAL REPORTS: Scientific and technical information considered important, complete, and a lasting contribution to existing knowledge.

TECHNICAL NOTES: Information less broad in scope but nevertheless of importance as a contribution to existing knowledge.

TECHNICAL MEMORANDUMS: Information receiving limited distribution because of preliminary data, security classification, or other reasons.

CONTRACTOR REPORTS: Scientific and technical information generated under a NASA contract or grant and considered an important contribution to existing knowledge.

TECHNICAL TRANSLATIONS: Information published in a foreign language considered to merit NASA distribution in English.

SPECIAL PUBLICATIONS: Information derived from or of value to NASA activities. Publications include conference proceedings, monographs, data compilations, handbooks, sourcebooks, and special bibliographies.

TECHNOLOGY UTILIZATION PUBLICATIONS: Information on technology used by NASA that may be of particular interest in commercial and other non-aerospace applications. Publications include Tech Briefs, Technology Utilization Reports and Notes, and Technology Surveys.

Details on the availability of these publications may be obtained from:

SCIENTIFIC AND TECHNICAL INFORMATION DIVISION

NATIONAL AERONAUTICS AND SPACE ADMINISTRATION

Washington, D.C. 20546